

## PERFORMANCE OF DEEP EXCAVATED RETAINING WALL IN SHANGHAI SOFT DEPOSIT

Z.H. Xu<sup>1</sup>, W.D. Wang<sup>2</sup>, J.H. Wang<sup>3</sup> and S.L. Shen<sup>4</sup>

**ABSTRACT:** This paper presents a field case of deep excavated pit of a building foundation in soft deposit of Shanghai lowland area. The details of the project are described at first. Then, the design method and construction process are presented. The wall displacements, axial force of struts, and displacement of the steel lattice columns were monitored and the results are presented and compared with the calculated results in design. Field measured data show that the ratio between the maximum lateral displacement and the excavated depth was controlled within 0.62%. Monitored data also show that the axial force in the second level struts was the largest among the three levels struts while the axial force in the first level strut was the smallest. The design method described in this paper is used to predict the diaphragm wall deformations. The prediction is consistent well with the measured data. However, there are some discrepancies of the axial forces in the struts between the calculated values and the measured values. Factors affecting effectiveness of the supporting system were investigated. The larger the thickness of the wall and the larger the stiffness of the struts, the smaller displacement of the wall will result. The rate of reduction of the wall displacement decreases with the increase of the thickness of the wall and the stiffness of the struts. There exists a threshold value of the depth ratio of the diaphragm wall, which has a significant influence on the lateral displacement. In this field case the threshold value of depth ratio is 0.3.

**Keywords:** Deep excavation, field monitoring, soft soil, diaphragm wall, design, construction

### INTRODUCTION

With the economic boom and infrastructure constructions in Shanghai, many areas in the city have been developed. There are more and more engineering projects of deep excavation for high-rise buildings in the city. Many excavation failures have occurred in this area and caused serious loss of property (Tang, 1999). Based on Tang's statistical report, 46 percent excavation problems were due to insufficient design considerations and 42 percent were caused by poor construction. This fact shows that reasonable design and construction are very important for successful excavation works. Design and construction of deep excavation is a challenging task for both geotechnical and structural engineers. This may be attributed to the lack of understanding of site-specific properties of soils and the mechanics of the interaction between the soil and the structure. In order to ensure safety in excavation works and protect the surrounding facilities, field monitoring becomes necessary. It can

monitor potential dangerous situations during the excavation process and measured data can check the design and guide construction. Many investigators have presented excavation case histories (Burland and Hancock, 1977; Mana and Clough, 1981; Finno, et al., 1989; Ou et al., 1993; Ou et al., 1998; Ng, 1998). Their studies helped to understand the characteristics of the wall deformation and the ground movement of the braced excavation in soft clay.

In this paper, the performance of a multi-propped deep excavation for a building (Shanghai Bank Building) foundation in Shanghai soft deposit is reported. The intention of this paper is to provide a detailed excavation record, which may help geotechnical engineers enhance the knowledge of the excavation behavior as well as the interaction between the soil and the structure in the soft deposit.

Design, construction, monitored performance during excavation, including lateral displacement of the retaining wall, settlement of the props and diaphragm

---

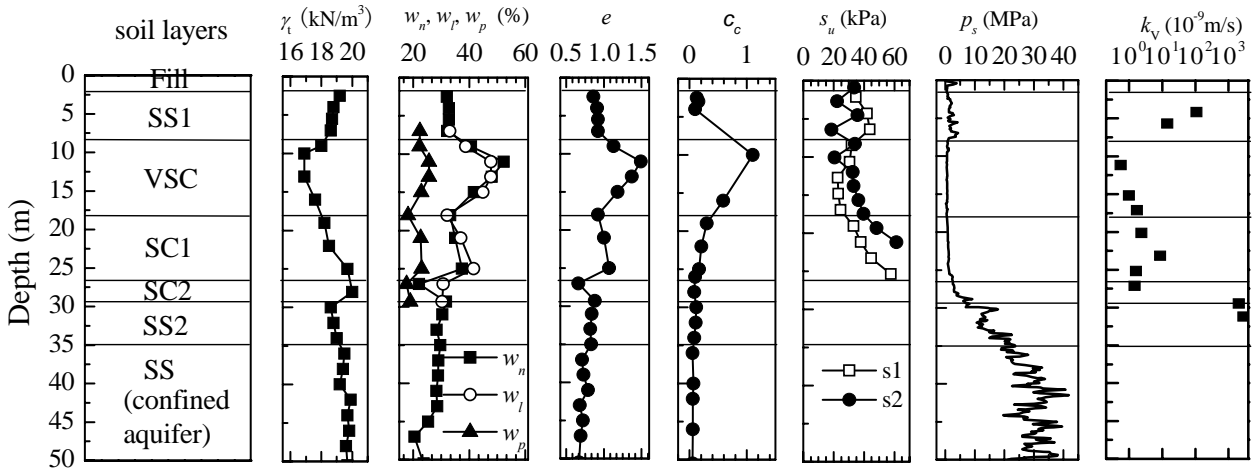
<sup>1</sup> Doctoral Student, Department of Civil Engineering, Shanghai Jiao Tong University, CHINA

<sup>2</sup> Senior Engineer, East China Architectural Design & Research Institute Co., Ltd., CHINA

<sup>3</sup> Professor, Department of Civil Engineering, Shanghai Jiao Tong University, CHINA

<sup>4</sup> Professor, Department of Civil Engineering, Shanghai Jiao Tong University, CHINA

*Note:* Discussion on this paper is open until June 30, 2006



Note:  $\gamma_t$ =unit weight,  $w_n$ =water content,  $w_p$ =plastic limit,  $w_l$ =liquid limit,  $e$ =void ratio,  $c_c$ =compressive index,  $s_u$ =field vane shear strength,  $p_s$ =tip resistance of CPT,  $k_v$ =hydraulic conductivity in vertical direction.

Fig. 1 Geotechnical profile and soil properties of the construction site

wall, and variation of the strut force are presented. Then, the design method is checked by comparing the calculated results with the measured values. Finally, factors affecting the effectiveness of the supporting system, the strengthening effectiveness of the soil-cement columns under the bottom of the excavated pit, and applicability of the design method are discussed.

### GEOTECHNICAL PROFILE AND SOIL PROPERTIES OF THE CONSTRUCTION SITE

The soft deposit at the excavated site is a deltaic sediment of Yangtze River. The elevation of the ground surface of the construction site is from 3.62 m to 4.32 m of Wusong Elevation System (Shanghai Geo, 1997). The groundwater table is 0.2 to 0.65 m from the ground surface. Figure 1 plots the geotechnical profile and soil properties of the borehole B4 (see Fig. 2) at the middle of the main building area. Field vane shear tests were performed at the boundary of the excavated area, as shown in Fig. 2. The top layer is a crust formed by backfill, including clay, gravel, cinder, and building rubbish with a thickness of about 2.2 m. Underlying is a deltaic-offshore deposit, called sandy silt (SS1) with a thickness of about 7.0 m. The soil of this layer is saturated with slight to medium dense and medium compressibility. The third layer beneath SS1 is very soft clay (VSC) with the average thickness of 9.0 m. The VSC layer contains mica, organic matter, and silty sand. It is in the saturated, high plastic, and high compressible state. The shear strength of this layer is quite low. The excavation was done till to this layer. The fourth layer is silty clay (SC1) with a thickness of about 7.5 m. It is in

the saturated, plastic, and medium compressible state. The fifth layer is also silty clay (SC2) with the average thickness of 2.8 m. It contains iron oxide spots and some organic matter. It is in the wet, medium to low plastic, and low compressible state. Under this layer is sandy silt (SS2) with the average thickness of about 5.0 m. It is in the saturated and medium dense state. Under SS2, it is silty sand (SS) with quite high CPT tip resistance  $p_s$ . The silty sand layer is the primarily confined aquifer in Shanghai. Hydrogeological investigation revealed that the pressure of the confined groundwater is 108 to 131 kPa. This pressure is almost equal to the self-weight of the soil under the basement bottom. As a result, special countermeasures should be taken into account to keep the stability of the bottom of the pit. The selection of appropriate countermeasures will be presented later in this study.

### PROJECT DESCRIPTION

Figure 2 shows the plan view of the excavated area. The building is mainly used for office spaces. It is composed of two parts—the main building at the south side and the annex building at the north side of the construction area. The main building is 46 stories and the annex building has 3 stories above the ground surface. The pile raft foundation is adopted for both parts and their basements are connected together. The thickness of the bottom slab of the main building is 3.2 m and the annex building is 1.0 m. The shape of the excavated pit is a regular square with an area of about 7,454 m<sup>2</sup>. The depth of the excavation at the main building is 17.15 m and at the annex building is 14.95 m. The total volume

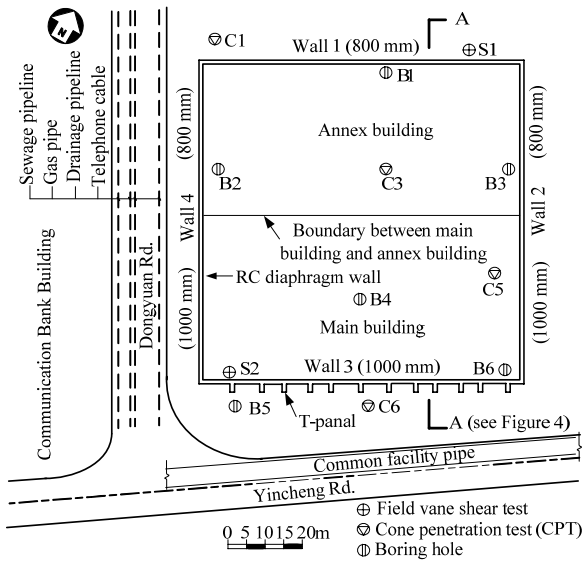


Fig. 2 Plan view of the excavated area

of the excavated soil is about 121,000 m<sup>3</sup>. The excavation was retained by reinforced concrete (RC) diaphragm wall with the thickness of 0.8 m and 1.0 m and the depth of 26.15 m to 32.5 m. Three levels of RC bracing structure were installed to strut the diaphragm wall. Many underground facilities including telephone cable, gas, drainage pipelines, sewage pipelines and common facility pipes were distributed around the excavated pit.

## EARTH RETAINING AND EXCAVATION WORK

### Selection of the Retaining System

To ensure the excavation work to be completed smoothly, a scheme with experienced design and construction method is necessary. According to the experience in Shanghai, diaphragm wall is a good selection for excavated retaining wall. The diaphragm wall has a relatively high stiffness as well as effective water sealing performance. Therefore, in this project, the diaphragm wall was adopted as the retaining wall as well as outside wall of the basement. Initially, it was planned that four levels of steel struts were adopted and the bottom slabs of the annex building and the main building were planned to be cast at different time. However, due to the much urgent construction time, this primary scheme was adjusted. Finally, supporting method using three levels of struts was used and RC struts rather than the steel struts were adopted since the former have higher stiffness. The bottom slabs of the annex building and the main building were planned to be cast at the same time. On the other hand, as the excavated depth of

the main building was greater than that of the annex building and wall 3 (see Fig. 2) had to bear heavier loads transferred from the main structure, a T-panel diaphragm wall was adopted for wall 3.

### Arrangement of Retaining Wall and Strut System

The arrangement of RC struts is plotted in Fig. 3. It was expected that with this arrangement, larger working space for the excavation is available. The struts were rigidly connected to the diaphragm wall via wales at each strut level. The sections of the bracing members are tabulated in Table 1. Blasting method was used to demolish the RC struts. Steel lattice columns (see Fig. 4) which were made up of four pieces of hot-rolling equilateral angle steel welded with tie plates were adopted as vertical props for supporting structures of this

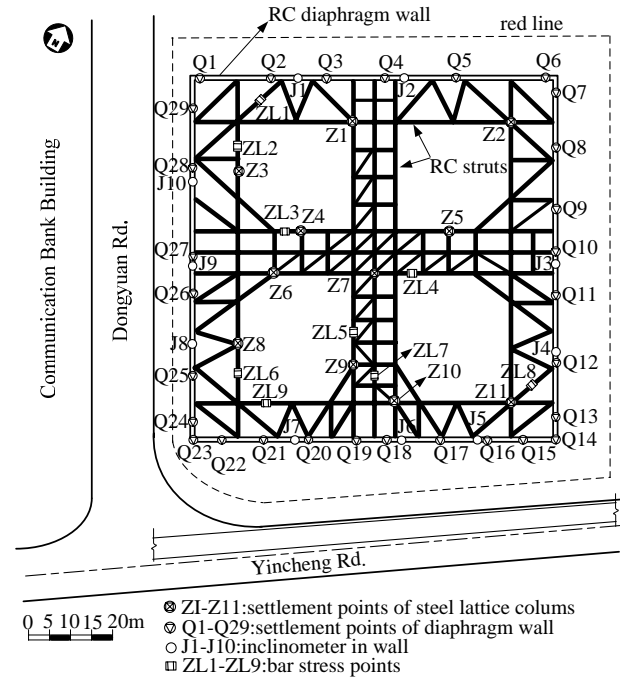


Fig. 3 Layout of supporting system and instrumentation

Table 1 Sections of bracing members

Levels	Bracing members	Sections
First level	Primary struts	900 × 700 mm
	Other struts	700 × 700 mm
	Wales	1200 × 800 mm
Second level	Primary struts	1200 × 700 mm
	Other struts	900 × 700 mm
	Wales	1400 × 800 mm
Third level	Primary struts	1200 × 700 mm
	Other struts	700 × 700 mm
	Wales	1400 × 800 mm

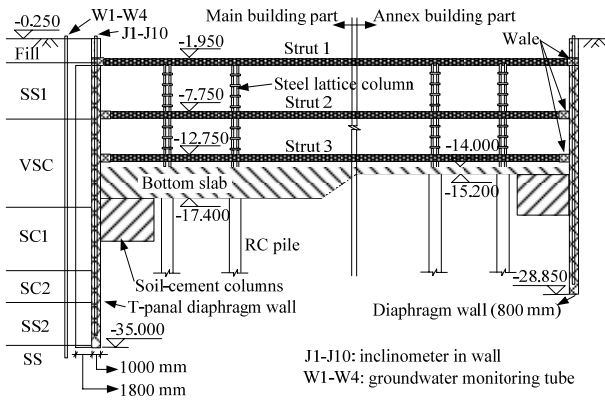


Fig. 4 Sectional view (section A-A) of excavated pit

project. After the excavation, concrete was cast around the steel lattice columns to form permanent columns. Figure 4 shows the sectional view of the excavated pit.

#### Installation of the Diaphragm Wall

Panel length of the diaphragm wall was 6.0 m. As sandy silt 1 (SS1) is prone to behave as a quick sand, the troughs may collapse during the wall installation. Therefore, before the wall installation, soil-cement columns were installed at the two sides of the troughs (see Fig. 5) to provide soil retention. The depth of the soil-cement columns for the diaphragm wall with width of 800 mm is 15.5 m while for the diaphragm wall with width of 1000 mm is 17.5 m.

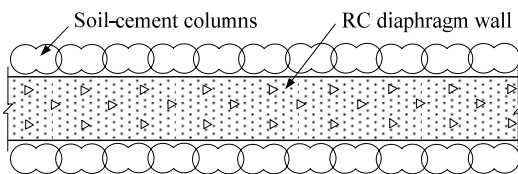


Fig. 5 Reinforcement of the trough (sectional view)

#### Excavation Procedure

Table 2 shows the schedule of the construction activities for this project. Construction of the RC diaphragm wall and the pile foundation began on June 1, 2002. The excavation started on August 10, 2002. The whole foundation work was completed on December 22, 2002. As shown in Table 2, stages 1, 2, 3, and 4 represent excavation stages. In order to reduce the wall displacement, careful countermeasures including layered and zoned excavation and bracing in time during planning and excavation were taken into consideration. The surcharge on the surface around the excavated pit never exceeded 20 kN/m<sup>2</sup>. Conveying of the excavated soil was via soil conveying path as shown in Fig. 6.

Table 2 Excavation sequences

Stage	Interval(d)	Construction activities
0	61	Construct diaphragm wall and pile foundation
1	10	Excavate to elevation of -2.7 m, install struts and wales at first strut level
2	22	Excavate to elevation of -8.5 m, install struts and wales at second strut level
3	16	Excavate to elevation of -13.5 m, install struts and wales at third strut level
4	10	Excavate to elevation of -15.2 m (annex building) and -17.4 m (main building)
5	31	Cast the bottom slab
6	9	Demolish the third level strut
7	18	Construct floor slab (B2F) at elevation of -9.5 m
8	9	Demolish the second level strut
9	9	Construct floor slab (B1F) at elevation of -5.5 m
10	9	Demolish the first level strut
11	11	Construct floor slab (1F) at elevation of ±0.000 m

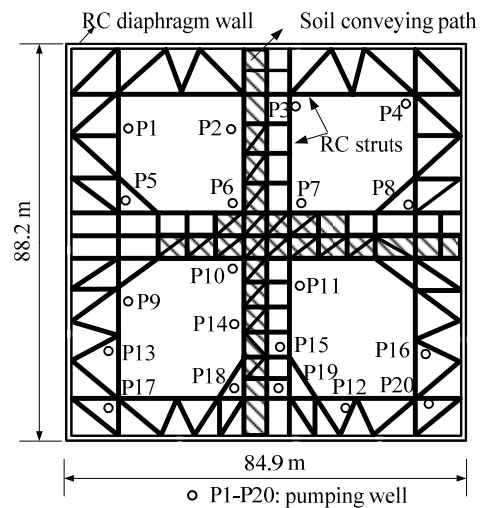


Fig. 6 Layout of soil conveying path and pumping wells

#### Soil-cement Columns and Groundwater Pumping

Eleven rows of soil-cement columns were used to strengthen a 6.2 m wide and 5.0 m deep soil zone under the bottom slab, as shown in Fig. 4. Each column was 0.7 m in diameter. The center to center spacing of columns was 0.5 m. This reinforcement had obviously improved the stability of the bottom of the excavated pit.

Groundwater was withdrawn throughout the excavation process only in the excavated pit using 20 wells. Figure 6 shows the location of these wells in the pit. The depth of the wells was about 20 m. The groundwater level was kept 1 m under the excavated surface during the excavation.

Field Monitoring

To monitor the behavior of the surrounding ground during the excavation, instrumentations were installed at various locations (see Fig.3). Field monitoring system includes the following aspects:

1. Monitoring displacements on retaining wall: 10 inclinometers (J1 to J10) were installed in the wall to monitor the lateral displacement of the diaphragm wall. 29 settlement points (Q1 to Q29) were setup to observe the vertical displacement at the top of diaphragm wall.
2. Monitoring settlements on strut system: 11 settlement points (Z1 to Z11) were setup to observe the vertical displacement of the steel lattice columns.
3. Monitoring axial forces of the struts: Rebar strain meters were installed in the struts to measure the strain of the rebar. All of the struts at each level (ZL1 to ZL9) were instrumented with rebar strain meters.

DESIGN APPROACH

Diaphragm Wall

The design method for the diaphragm wall was proposed by ACECS (1997). It follows the procedure as presented by Xiao et al. (2003), which is based on the elastic subgrade theory. The calculation model is shown in Fig. 7. In this model, the diaphragm wall is modeled as a beam, the ground is modeled as a set of Winkler

springs, and the bracings are also modeled as springs. Moreover, lateral pressure distributions are taken as triangular above the excavated plane while rectangular under the excavated plane. In the calculation, the lateral pressures are evaluated by the sum of the water pressure and earth pressure. By selecting a unit length of the diaphragm wall, the flexural differential equations of the diaphragm wall are as follows:

$$EI \frac{d^4 y}{dz^4} - e_a(z) = 0 \quad (0 \leq z \leq h_n) \quad (1)$$

$$EI \frac{d^4 y}{dz^4} + m(z - h_n)y - e_a(z) = 0 \quad (z \geq h_n) \quad (2)$$

where  $EI$ = flexural rigidity of the diaphragm wall,  $y$ = lateral displacement of the diaphragm wall,  $z$ =depth,  $e_a(z)$ = distribution function of Rankine's active earth pressure considering the surcharge  $q=20 \text{ kN/m}^2$ ,  $m$ = modulus of horizontal subgrade reaction,  $h_n$ =excavated depth of  $n$ th stage.

As the soil is layered and there are some bracings, we have to separate the diaphragm wall into several sections. For each section, the flexural differential Equation (1) or (2) are established. Finite element method is then adopted to solve the equations.

The reaction forces of the bracing springs can be calculated as follows:

$$T_i = K_{Bi}(y_i - y_{0i}) \quad (3)$$

where  $T_i$ =the reaction force of the  $i$ th level bracing spring,  $K_{Bi}$ =the axial stiffness of the  $i$ th level bracing,  $y_i$ =the lateral displacement of the  $i$ th level bracing spring calculated at the current stage,  $y_{0i}$ =the lateral displacement of the  $i$ th level bracing spring calculated at the last stage.

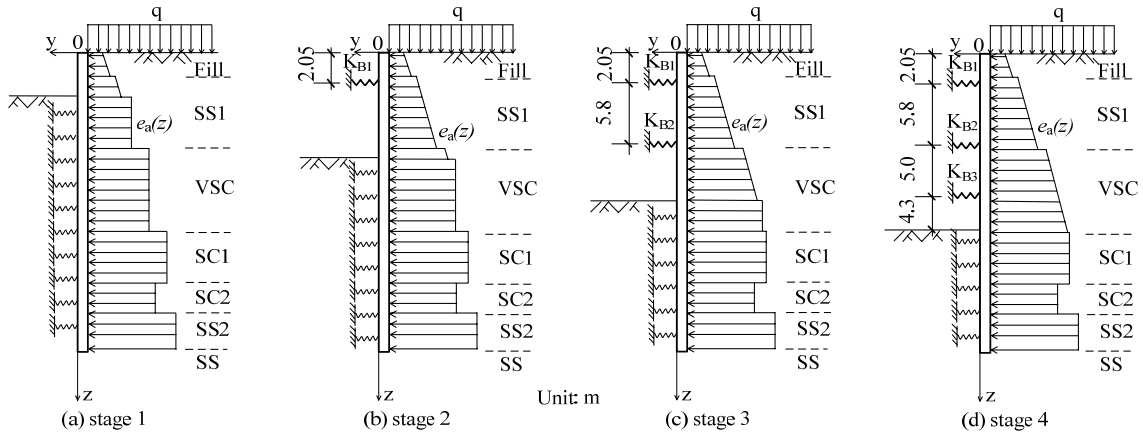


Fig. 7 Calculation model of diaphragm wall in various stages

Calculation of Bracing Axial Stiffness  $K_{Bi}$

For the bracing system which is composed of cross-lot braces and wales, the theoretical value of the stiffness of the supports can be defined in terms of its axial stiffness,  $K_{Bi}$ :

$$K_{Bi} = EA/SL \tag{4}$$

where  $A$  is the cross-sectional area of the bracing,  $E$  is the elastic modulus of the bracing,  $L$  is the half of the bracing length, and  $S$  is the horizontal distance between bracings. However, for a complicated bracing system, Equation (4) may not give reasonable stiffness value. Since the bracing members including the struts and wales at the same level form a plane bar system, a simple method to calculate the equivalent stiffness of the bracing system is as follows:

$$K_{Bi} = p/\delta \tag{5}$$

where  $p$  is the uniform load acting on the wales ( $p=1N/m$ ) and  $\delta$  is the mean displacement of the intersections between the wales and struts caused by  $p$ .

Figure 8 depicts the calculation model of  $\delta$ . A tie bar which fixes the  $x$ -displacement is added at point A and another two tie bars which fix the  $y$ -displacement are added at point B and point C. These three tie bars are added to fix the rigid body motion of the system. Plane bar system FEM is then adopted to calculate the displacements of the intersections between the wales and the struts.  $\delta$  is obtained by calculating the mean displacement of these intersections. In the calculation, the value of Yang's modulus  $E$  for all the concrete bracing members is  $3 \times 10^{10} N/m^2$  and the sections of the bracing members are listed in Table 1.

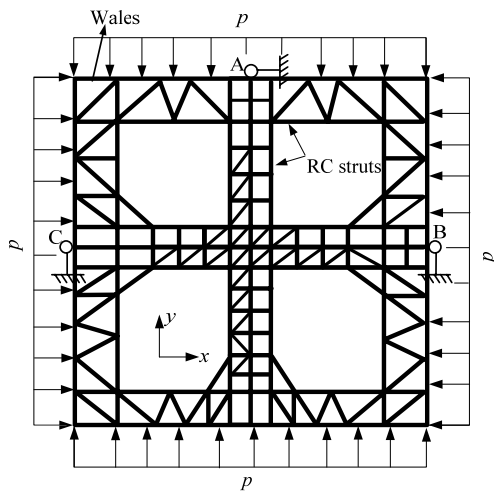


Fig.8 Calculation model of  $\delta$

Based on Equation (5), the equivalent stiffness of the first level bracing  $K_{B1}$  is  $39.68 MN/m^2$ , whereas those of the second and third level bracing are  $K_{B2} = K_{B3} = 52.36 MN/m^2$ .

Bracing Members

The reaction force calculated from Equation (3) is acted on the wales and then plane bar system FEM is adopted to calculate the internal forces of the bracing members. The calculation model is shown in Fig.8.

Parameters Used in the Calculation

Table 3 gives the parameters for the in situ soil and soil-cement columns. Cohesion  $c$  and angle of internal friction  $\phi$  were obtained from the direct shear test. The modulus of horizontal subgrade reaction  $m$  was obtained from the experience in Shanghai, based on the soil type (ACECS, 1997).

Table 3 Design parameters in the calculation

Materials	$\gamma$	$c$	$\phi$	$m$	$s_u$
Fill	18.0	0.0	22.0	1.0	34.0
SS1	18.8	5.0	30.0	2.0	32.3
VSC	17.2	14.0	11.0	1.0	29.0
SC1	18.5	12.0	19.0	2.0	48.2
SC2	20.0	51.0	18.0	4.0	102.0
SS2	18.9	4.0	30.0	4.0	
SS	19.2	1.0	36.0	6.0	
Soil-cement columns	20.0	16.0	25.0	4.0	

Note:  $\gamma$ =unit weight ( $kN/m^3$ ),  $c$ =cohesion (kPa),  $\phi$ =angle of internal friction ( $^\circ$ ),  $m$ = coefficient of modulus of horizontal subgrade reaction ( $MN/m^4$ ),  $s_u$ =undrained shear strength (kPa)

FIELD MEASURED RESULTS

Lateral Displacements

Figure 9 depicts the lateral displacement in the diaphragm wall at stages 2, 3, 4, and 5 (see Table 2) which are the main excavation stages. Furthermore, the lateral displacement in diaphragm wall at stage 11 was also given. It can be seen that during the excavation the lateral displacement increases gradually with excavated depth before completion of the bottom slab. The maximum lateral displacement of wall 1 was 93.06 mm at the depth of 14.0 m and it was occurred at inclinometer J1 at stage 5. The ratio between the

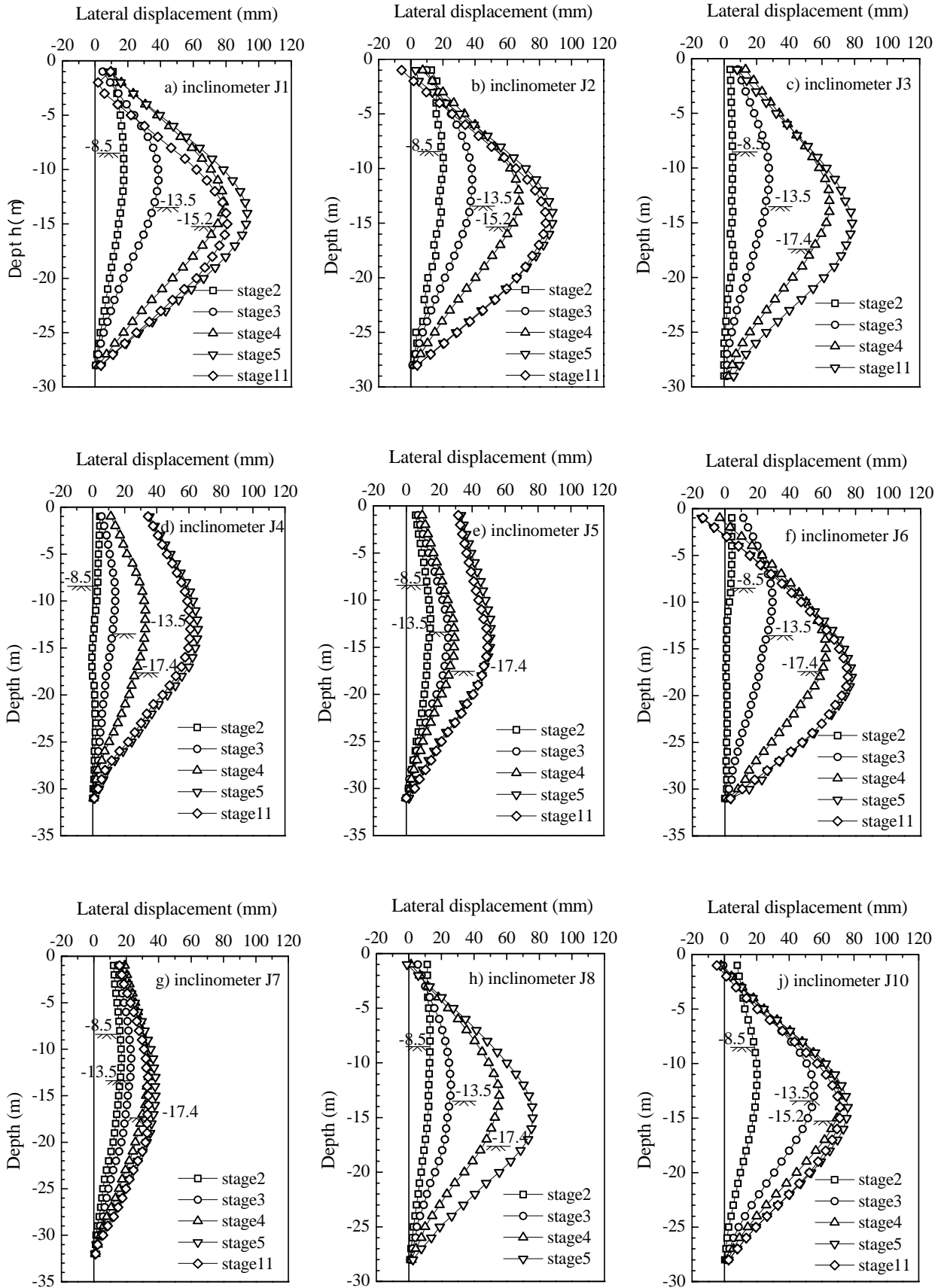


Fig. 9 Lateral displacement of diaphragm wall at the end of main stages

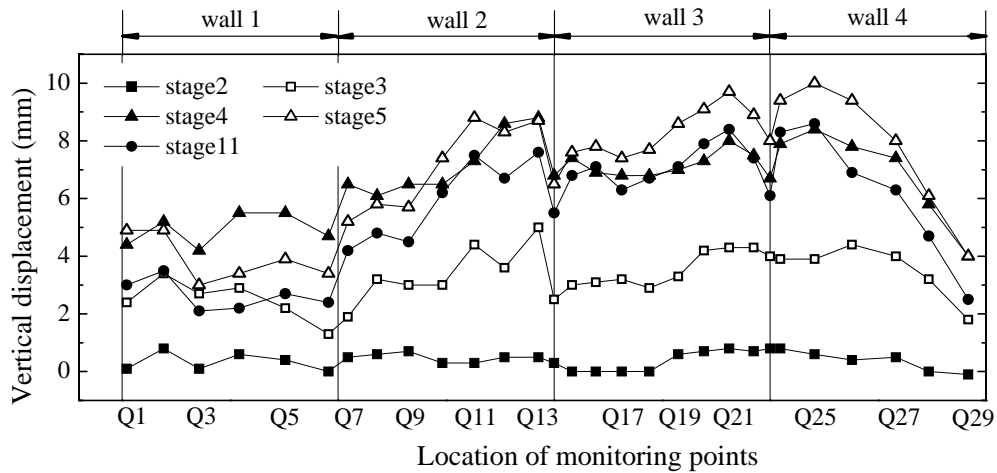


Fig. 10 Vertical displacement at the top of diaphragm wall

maximum lateral displacement of wall 1 and the excavated depth is 0.62%. The maximum lateral displacement of wall 3 was 77.75 mm at the depth of 18.0 m and it was occurred at inclinometer J6 at stage 5. The ratio between the maximum lateral displacement of wall 3 and the excavated depth is 0.45%. The minimum lateral displacement was 38.16 mm at the depth of 15.0 m and it was occurred at inclinometer J7 at stage 5. The ratio between the minimum lateral displacement and the excavated depth is 0.22%. It took 31 days to cast the bottom slab. During this time (from the end of stage 4 to the end of stage 5, see Table 2), all of the inclinometers had noticeable lateral displacement increment as shown in Fig. 9. This may be caused by the creep property of the soft soil as well as consolidation.

#### Vertical Displacements of the Wall

Figure 10 shows the vertical displacement at the top of the diaphragm wall. It can be seen that the diaphragm wall was uplifted during excavation. The maximum vertical displacement was 10 mm occurred at Q25 at stage 5. Moreover, the vertical displacement of the wall at the annex building was quite smaller than that at the main building. This is because the depth of excavated ground where the main building is located was larger than that at the annex building. The vertical displacement at Q14 and Q23 was smaller than that at their neighboring points. This may be because Q14 and Q23 were located at the corners of the wall.

#### Vertical Displacements of Steel Lattice Columns

Figure 11 depicts the vertical displacement of steel lattice columns. Steel lattice columns were also uplifted

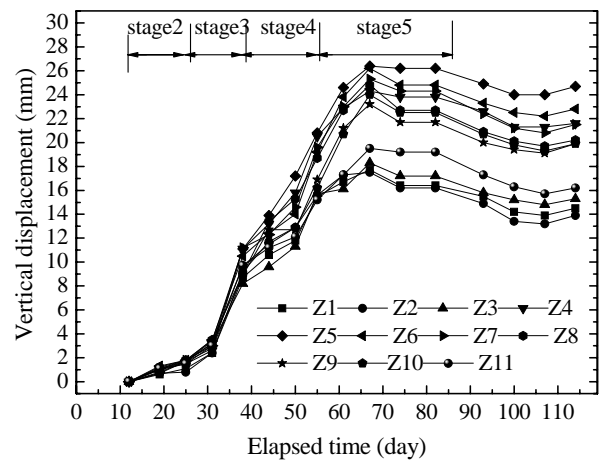


Fig. 11 Vertical displacement of steel lattice columns

as the diaphragm wall behaved. The maximum vertical displacement was 20.8 mm occurring at Z5 at stage 4. The vertical displacement at Z4, Z5, Z6, and Z7 was much larger than that at Z1, Z2, Z3, and Z11. This is because that Z4, Z5, Z6, and Z7 were located at the center of the pit while Z1, Z2, Z3, and Z11 were near the corners of the excavated pit. Furthermore, there was a different uplift among the steel lattice columns. At stage 2, the different uplift was quite small. However, it increased with the excavation process. The maximum different uplift was 5.6 mm at stage 5.

#### Axial Forces in the Struts

Figure 12 depicts the axial force in the concrete struts. Axial force in the second level strut was the largest among the three level struts while axial force in the first level strut was the smallest. The maximum axial force occurred at the same plan position of ZL8 (see Fig. 3)

which was at the corner of the pit. The maximum axial force in the first level strut was 7.6 MN at ZL8-1, whereas in the second level strut was 16.6 MN at ZL8-2, and in the third level strut was 14.1 MN at ZL8-3. It can also be seen that the axial force increased with the excavation as well as the lateral displacement. After the excavation finished, the axial force in most of the struts of the first and second level became stable. However, after the construction of the bottom slab, axial force in most of the struts of the third level decreased. The reason may be that the bottom slab began to share loads transferred from the diaphragm wall.

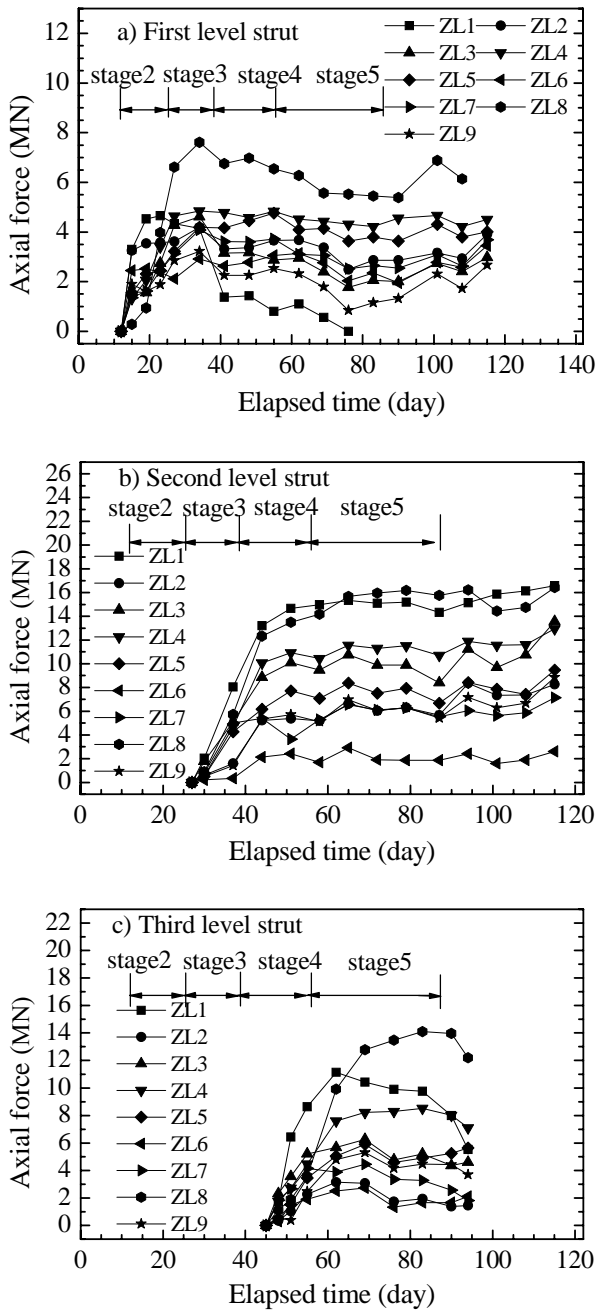


Fig. 12 Variation of axial force in struts

COMPARISON BETWEEN MEASURED AND CALCULATED VALUES

Lateral Displacements of Diaphragm Wall

The measured lateral displacements of the wall in the annex building and in the main building at stage 4 (excavate to the full depth) are compared with the calculated data, as shown in Fig. 13. It can be seen that the calculated deformation shapes agree well with the measured values. The maximum calculated displacement is 69.0 mm (comparing to measured value of 67.44 mm) for the annex building and the maximum displacement for the main building is about 40.7 mm (comparing to measured value of 33.9 mm). This shows that the design method based on the elastic subgrade theory can give reasonable prediction of the lateral displacement of the diaphragm wall.

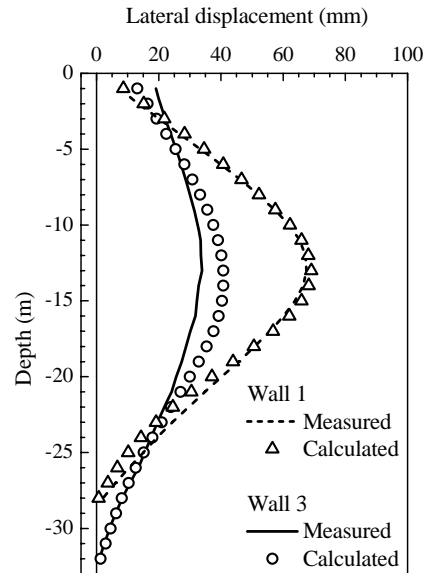


Fig. 13 Comparison of measured and calculated lateral displacement at stage 4

Axial Force in Struts

A comparison between the calculated and the maximum measured axial force in the three levels struts is shown in Fig. 14. It can be seen that the calculated values are consistent with the measured value fairly well. The axial force in ZL2-6 is over-predicted by a maximum scale of 80.66%. However, for other struts whose axial force is over-predicted, the over-predicted scale is within 2.59% to 41.2%. For those struts whose axial force is less-predicted, the less-predicted scale is within 6.4% to 40.16%.

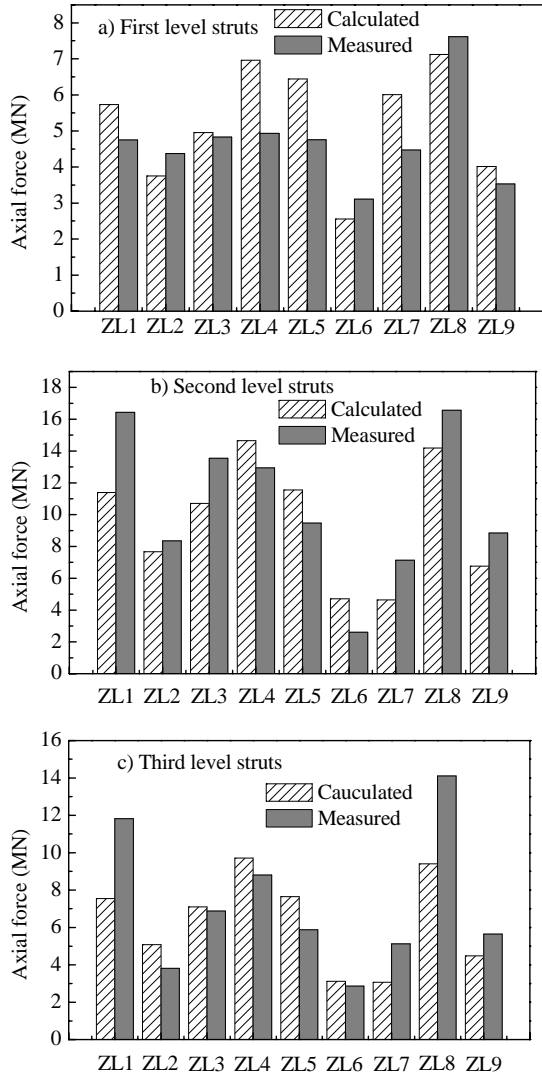


Fig. 14 Comparison of measured and calculated axial force in struts

There are many factors contributing to the difference between the measured and the calculated axial force in the struts. These factors include measuring error, temperature effect, and creep property of the concrete. Moreover, the nonlinear stress-strain behavior of the concrete of the struts was not considered.

Predictions of Lateral Displacement with Clough and O'Rourke's Charts (1990)

Clough and O'Rourke (1990) proposed charts (see Fig. 15) to predict the maximum lateral displacement of a diaphragm wall supporting systems in clays. The prediction is based on the relative stiffness of the wall and FS (the factor of safety against basal heave) which is defined by Terzaghi (1967). Calculation method for FS is given in Fig. 16. Parameters used to calculate the FS are listed in Table 3. It should be pointed out that the 7th

soil layer SS is considered as hard stratum for calculating the FS as it has relative higher shear strength. The calculated FS in full excavated depth for wall 1 and wall 3 are 1.32 and 1.36, respectively. For all the diaphragm wall, the value of Yang's modulus  $E$  is  $3 \times 10^{10}$  N/m<sup>2</sup>. The relative stiffness of wall 1 is 374 and of wall 3 is 712. According to the calculated relative stiffness and the FS, Fig. 15 gives the prediction of the ratio between the maximum lateral displacement and excavated depth of wall 1 and wall 3. The predicted value of wall 1 is 0.54% (comparing to the measured value of 0.62%) while the predicted value of wall 3 is 0.46% (comparing to the measured value of 0.45%). Both the predicted lateral displacement of wall 1 and wall 3 agree well with the measured values. This indicates that the charts can be used to give reasonable estimates for movements of the wall in Shanghai soft soil.

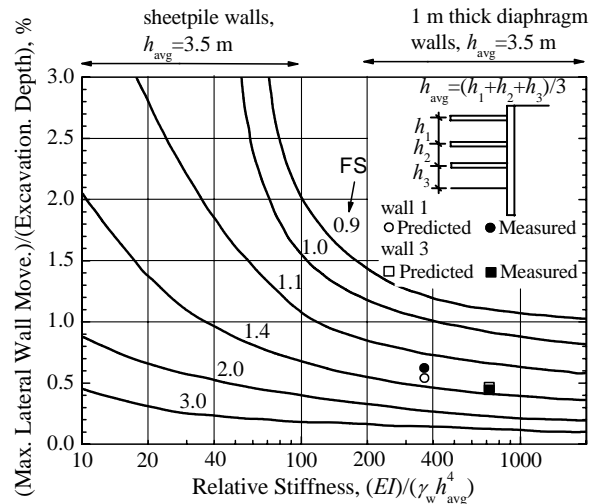


Fig. 15 Charts for predicting wall movements (based on Clough and O'Rourke 1990)

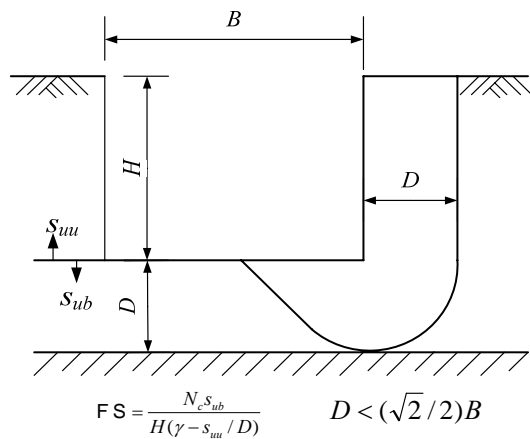


Fig. 16 Factor of safety against basal heave (Terzaghi, 1967)

## DISCUSSION

### Factors Affecting Effectiveness of the Supporting System

In addition to geotechnical and construction influences on effectiveness of the supporting system, the thickness of the diaphragm wall, the stiffness of the struts, and the ratio of the embedded length under the bottom of the excavated pit to the excavated depth (depth ratio of the diaphragm wall) can also have significant influences. The latter factors are particularly significant because they can be controlled by the designer. It is important to utilize these factors to improve the effectiveness of the supporting system while at the same time to be able to realize the limitations of their influence.

#### Thickness of the Diaphragm Wall

Figure 17 shows the relationship between the calculated maximum lateral displacement and the thickness of wall 3. It can be seen that the thickness of the diaphragm wall has obvious influence on the displacement of the wall. The larger the thickness of the wall, the smaller displacement will result. However, the rate of reduction of the wall displacement decreases with the increase of the thickness of the wall. This indicates that it is important to select the appropriate thickness of the diaphragm wall which can effectively control the wall deformation as well as the cost of the wall.

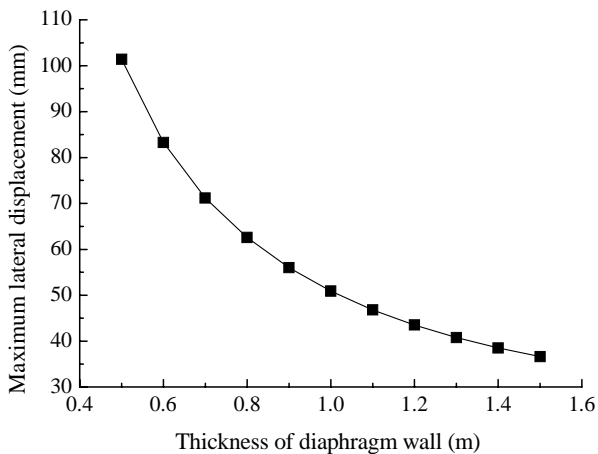


Fig. 17 Relationship between the calculated maximum lateral displacement and the thickness of wall 3

Though the excavated depth of the annex building was shallower than that of the main building, the maximum lateral displacement at inclinometer J1 and J2 were much larger than that of the inclinometers J4 to J8.

This is because the thickness of the diaphragm wall in the main building is much larger than that in the annex building. Moreover, T-panel diaphragm wall can effectively reduced the lateral displacement of the diaphragm wall as it has higher stiffness. As can be seen in Fig. 9, the lateral displacement in the inclinometers J5 and J7 were much smaller than that in the other inclinometers.

#### Stiffness of the Struts

Figure 18 shows the relationship between the calculated maximum lateral displacement of wall 3 and the stiffness ratio of the struts  $R_E$  which is defined in the inset of this figure. The maximum lateral displacement in Fig. 18 is calculated using the same  $R_E$  among the three levels struts. The change tendency between the maximum lateral displacement and  $R_E$  is somewhat like that between the maximum lateral displacement and the thickness of the diaphragm wall. It can also be seen that the larger the stiffness of the struts, the smaller the displacement will result. However, the rate of reduction of the wall displacement decreases with the increase of the stiffness of the struts.

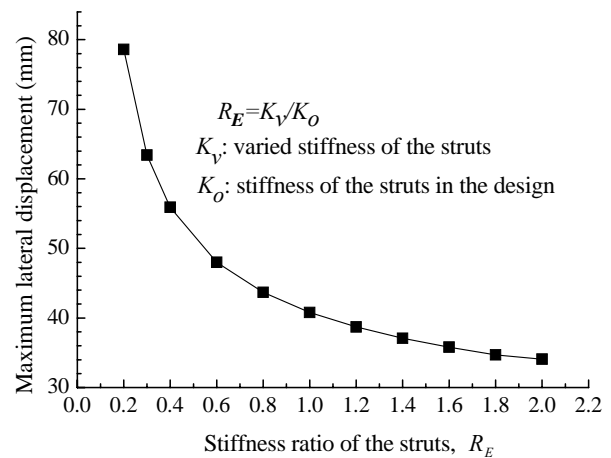


Fig. 18 Relationship between the calculated maximum lateral displacement and the stiffness ratio of the struts

#### Depth Ratio of the Diaphragm Wall

The relationship between the calculated maximum lateral displacement and the depth ratio  $R_H$  of wall 3 is shown in Fig. 19. When  $R_H$  is 0.3 (the corresponding embedded length under the bottom of the excavated pit is 6.86 m), the calculated maximum lateral displacement is 44.3 mm. While  $R_H$  increases to 1.4 (the corresponding embedded length under the bottom of the excavated pit is 24 m), the calculated maximum lateral

displacement reduces to 40.5 mm by a small scale of 9.4%. This indicates that if  $R_H$  is larger than 0.3, it has little influence on the lateral displacement of the diaphragm wall. However, if  $R_H$  is smaller than 0.3, reducing the depth ratio will lead to dramatic increase in maximum lateral displacement. On the other hand, a very small depth ratio may cause base instability.

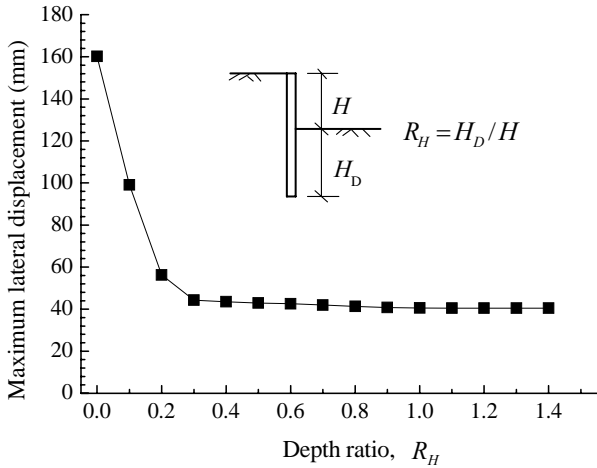


Fig. 19 Relationship between the calculated maximum lateral displacement and the depth ratio

#### Effectiveness of the Soil-cement Columns for Base Stability

The soil-cement columns which are used to strengthen the soil under the bottom of the excavated pit may increase the modulus of horizontal subgrade reaction  $m$  of the soil at the strengthened zone. Figure 20 depicts the relationship between the calculated maximum

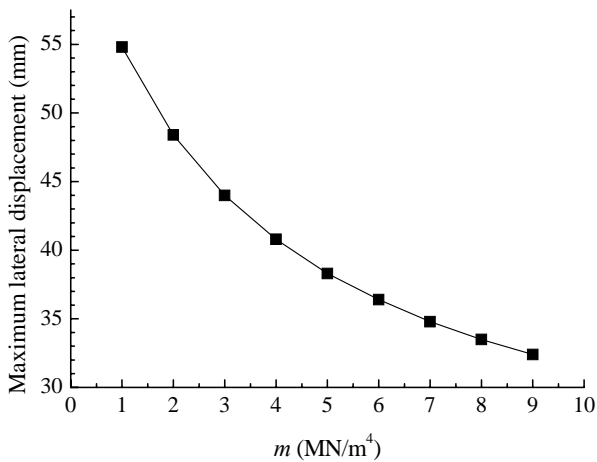


Fig. 20 Relationship between calculated maximum lateral displacement and  $m$  of the soil at the strengthened zone under the bottom of the excavated pit

lateral displacement of wall 3 and  $m$ . When  $m=1 \text{ MN/m}^4$  which means that the soil under the bottom of the excavated pit is not strengthened, the calculated maximum lateral displacement is 54.8 mm. When  $m$  increases to  $4 \text{ MN/m}^4$ , the maximum lateral displacement reduces to 40.8 mm by a scale of 25.5%. This means that the soil-cement columns under the bottom of the excavated pit can effectively control the wall deformation. However, the rate of reduction of the wall displacement decreases with the increase of the  $m$  value.

#### Applicability of the Design Method

Terzaghi (1967) found that a wall movement of the order of 0.001 times the wall height is sufficient to make the soil at the back of the wall into active state while much larger movements are requested to develop the passive state. Subsequent experiment and theoretical studies (Clough and Duncan, 1971) have confirmed this statement. Lee et al. (1983) summarizes many experiment results and points out that movement – wall height ratio to develop the passive state is found to vary from 1% to 6.4%. A large numbers of testing results of foundation pits in soft soil (Long, 2001, see Table 3 and Table 4) have demonstrated that the ratio of movement towards the pit to the excavated depth is larger than 0.1%. However, under the excavated depth, the ratio of movement towards the pit to excavated depth rarely reaches 1%. This means that the soil at the back of the wall can reach active state while the soil in front of the wall is usually under passive state. Therefore, it is reasonable to use Rankine’s active earth pressure theory to calculate the lateral pressure at the back of the wall while modeling the soil in front of the wall as a set of Winkler springs.

The calculation method based on the elastic subgrade theory is widely used by engineers in Shanghai. This analysis method can calculate the forces and displacements of the diaphragm wall at various excavation stages. It is important to select appropriate values for mechanical parameters in the theoretical predictions.

#### CONCLUSIONS

This paper presents a case history of the field behavior of the multi-propped deep excavation for a building foundation in Shanghai urban area. The following conclusions can be drawn:

1. The ratio between the maximum lateral displacement and the excavated depth was controlled in

0.62%. During the stage of casting the slab, wall deflection increased obviously with time while the excavated depth kept unchanged. The lateral displacement in wall 3 was relatively small even though the excavated depth in the main building was much larger than that in the annex building. This shows that the T-panel diaphragm wall is effective for reducing the wall deflection.

2. Design method based on the elastic subgrade theory was reasonable to calculate the diaphragm wall. Comparison between the calculated and the measured results has shown that this calculation method can give good prediction of the diaphragm wall deformations. The axial force obtained by the proposed method is fairly close to the measured data.

3. Predictions of the lateral displacement of the diaphragm wall using Clough and O'Rourke's charts are consistent with the measured values.

4. There is a threshold value of the depth ratio  $R_H$  that affects the lateral displacements of the diaphragm wall significantly. In the present case, this value is 0.3. When  $R_H$  is less than 0.3, very large wall displacements will occur. However, when  $R_H$  is over this threshold values, it do not have significant influence on the lateral displacements.

#### ACKNOWLEDGEMENTS

The authors would like to express their sincere thanks to Shanghai Geotechnical Investigations & Design Institute and Shanghai Zhongpu Investigation Institute for their field data.

#### REFERENCES

- Association of Civil Engineering Consultants in Shanghai (ACECS) (1997): Shanghai Standard Code for Design of Excavation Engineering-DBJ08-61-97, Shanghai, 159p. (in Chinese).
- Burland, J. B., and Hancock, R.J.R. (1977). Underground carpark at the House of Commons, London: Geotechnical aspects. *Struct. Engr.*, 55 (2): 87-100.
- Clough, G.W., and Duncan, J. M. (1971). Finite element analysis of retaining wall behavior. *Journal of the Soil Mechanics and Foundations Division*, 97 (12): 1657-1673.
- Clough, G.W., and O'Rourke, T.D. (1990). Construction induced movements of in situ walls. *Proc., ASCE Conf. on Des. and Perf. of Earth Retaining Struct., Geotech. Spec. Publ. No. 25*, ASCE, New York, 439-470.
- Finno, R.J., Atmatzidis, D.K., and Perkins, S.B. (1989). Observed performance of a deep excavation in clay. *J. Geotech. Engrg.*, ASCE, 115 (8): 1045-1064.
- Lee, I.K., White W., and Ingles, O.G. (1983). *Geotechnical engineering*, Massachusetts: Pitman Publishing Inc..
- Long, M. (2001). Database for retaining wall and ground movements due to deep excavations. *J. of Geotech. and Geoenviron. Engrg.*, ASCE, 127 (3): 203-224.
- Mana, A.I., and Clough, G.W. (1981). Prediction of movements for braced cut in clay. *J. Geotech. Engrg. Div. ASCE*, 107 (8): 759-777.
- Ng, C.W.W. (1998). Observed performance of multipropped excavation in stiff clay. *J. Geotech. Engrg.*, ASCE, 124 (9): 889-905.
- Ou, C.Y., Hisieh, P.G., and Chiou, D.C. (1993). Characteristics of ground surface settlement during excavation. *Can. Geotech. J.*, Ottawa, Canada, 30 (5): 758-767.
- Ou, C.Y., Liao, J.T., and Lin, H.D. (1998). Performance of diaphragm wall constructed using top-down method. *J. Geotech. Engrg.*, ASCE, 124 (9): 798-807.
- Shanghai Geotechnical Investigations & Design Institute (Shanghai Geo) (1997): *Geotechnical investigation report of Shanghai Bank Building*. 120p. (in Chinese).
- Tang, Y.Q., Li, Q.M., and Cui, J.Y. (1999). Analysis and treatment of excavation failures. *Chinese Architecture & Building Press*, Beijing, 543p. (in Chinese).
- Terzaghi, K (1967). *Theoretical Soil Mechanics*, New York: John Wiley & Sons.
- Xiao, H.B., Tang, J., Li, Q.S., and Luo, Q.Z. (2003). Analysis of multi-braced earth retaining structures. *Structures & Buildings*, ICE, 156 (SB3):307-318.